Single-Particle Photoluminescence Spectra, Blinking, and Delayed Luminescence of Colloidal $CuInS_2$ Nanocrystals

Patrick J. Whitham, Arianna Marchioro, Kathryn E. Knowles,

Troy B. Kilburn, Philip J. Reid,* and Daniel R. Gamelin*

Department of Chemistry, University of Washington, Seattle, WA 98195-1700, USA

**Electronic address: gamelin@chem.washington.edu, pjreid@uw.edu*

Abstract. Single-nanocrystal and ensemble photoluminescence measurements on $CuInS_2$ semiconductor nanocrystals reveal intrinsically broad luminescence bandshapes attributable to strong electron-phonon coupling in the emissive excited state, similar to the single-nanocrystal luminescence spectra of Cu^+-doped CdSe nanocrystals. This finding is consistent with the hypothesis of exciton self-trapping in $CuInS_2$ NCs, which forms an emissive state similar to those of Cu^+-doped nanocrystals. Blinking is observed that resembles that of other semiconductor nanocrystals. Ensemble luminescence measurements reveal the existence of a remarkably long-lived excited state in these nanocrystals that continues to emit photons over several orders of magnitude in time following the excitation pulse. This delayed luminescence is attributed to reversible electron trapping. The delayed luminescence overlaps in time and shows similar distributed kinetics to the blinking "off" times, supporting the proposal that these two phenomena arise from the same microscopic carrier-trapping and -detrapping processes. Excitation power dependence measurements illustrate that the delayed luminescence saturates at very low intensities at the power densities used in single-nanocrystal measurements, consistent with this metastable charge-trapped state being the "off" state of the luminescence blinking cycle.

Introduction

$CuInE_2$ (E = S, Se, Te) nanocrystals (NCs) have recently attracted a great deal of interest as nontoxic alternatives to CdSe, PbS, and related semiconductor NCs for numerous nanophosphor applications.[1-3] The large photoluminescence (PL) Stokes shifts and long lifetimes of $CuInE_2$ NCs make them particularly attractive emitters for applications in bioimaging,[2, 4] light-emitting diodes,[5] and luminescent solar concentrators.[6-8] Compared to II-VI or IV-VI semiconductor NCs such as CdSe and PbS, however, the luminescence mechanism in $CuInE_2$ NCs is not very well understood.

Bulk $CuInS_2$ displays several distinct PL transitions including free-exciton emission, free-to-bound recombination, and donor-acceptor pair (DAP) recombination.[9-12] A narrow near-band-edge emission feature is observed at 1.53 eV (~50 meV full-width at half maximum (fwhm) at 300 K), and broader deep-trap emission is observed between 1.3 and 1.4 eV.[9, 11] The free-to-bound and DAP recombination processes are generally interpreted as involving lattice vacancies or other point defects. The specific PL spectrum displayed by bulk $CuInS_2$ thus depends on the methods of crystal growth and post-growth annealing, which affect the concentrations of such defects, ranging from $10^{13} – 10^{20}$ per cm^3 in $CuInS_2$ depending on preparation conditions.[13-14]

$CuInS_2$ NCs are dominated by a broad mid-gap PL feature (~300 – 400 meV fwhm at 300 K)[15] that exhibits a large Stokes shift of ~250 – 500 meV and that bears little resemblance to the characteristic PL features of bulk $CuInS_2$.[16] The energy of this broad PL can be tuned by changing the NC size.[15, 17-22] Various mechanisms have been proposed to explain this PL. Most proposed mechanisms are analogous to those discussed for bulk $CuInS_2$, and invoke lattice vacancies or interstitials to generate DAP or free-to-bound recombination processes similar to bulk.[17, 20, 23-25] Extrapolating the bulk concentration of defects to the nanoscale would give values

equivalent to greatly less than one and up to 10 defects per NC depending on size. Therefore, in the low concentration limit DAP emission is less likely to be observed. Evidence for DAP recombination in $CuInS_2$ NCs includes a PL red shift on the 100 ns time scale observed in gated measurements.[20, 26] This PL red shift has been explained as coming from a distribution of donor/acceptor distances.[20, 26] Elsewhere, the same red shift has been interpreted instead in terms of size-dependent surface trapping kinetics.[25, 27] In all of these interpretations, the broad PL bandshape is either explicitly or implicitly attributed to inhomogeneous broadening. In stark contrast with bulk, the PL of $CuInS_2$ NCs is remarkably robust with respect to NC defects. While the peak energies and quantum yields have been reported to vary with stoichiometry,[23, 28] the key features of large bandwidths and large Stokes shifts remaining largely unchanged from nearly stoichiometric or copper-rich to severely copper deficient compositions.[24, 29]

Recently, two alternative proposals have also suggested the possibility that $CuInS_2$ NC PL can be explained without invoking lattice defects. A theoretical study based on the multi-band effective-mass approximation proposes the existence of large Stokes shifts and long PL lifetimes in quantum-confined $CuInS_2$ NCs stemming from the first-order forbiddenness of the lowest-energy inter-band electronic transition, which becomes partially allowed through low-symmetry effects.[30] In this interpretation, absorption is dominated by higher-energy band-like excitonic states, but PL occurs *via* this low-energy forbidden state, generating a large Stokes shift. The large experimental PL bandwidths in this scenario would result from inhomogeneous broadening within an ensemble of NCs.

The second recent proposal is that $CuInE_2$ NC PL involves exciton self-trapping.[15] This mechanism accounts for both the large Stokes shifts and the broad bandshapes observed in the PL of $CuInE_2$ NCs by invoking strong excited-state vibronic coupling. This interpretation has

been proposed to explain the PL of $CuInE_2$ NCs based on similarities in PL bandwidths, lifetimes, Stokes shifts, and magnetic-field dependence between $CuInS_2$ and Cu^+-doped semiconductor NCs.[15-16] In the latter, photogenerated holes localize around individual Cu^+ dopant ions, causing large lattice distortion at this localization site.

Single-particle spectroscopy can provide new insight into the mechanism of PL in $CuInS_2$ NCs by evaluating ensemble particle-size heterogeneity as a source of spectral inhomogeneous broadening. Inhomogeneous particle sizes account for only a small portion of the ensemble PL bandwidths of Cu^+-doped NCs,[31-33] but to date, there have been no reports of any single-particle spectra for any $CuInE_2$ NCs. PL blinking has been reported for single copper-doped Zn-In-S alloyed NCs,[34] but single-particle PL spectra were not reported.

In addition to resolving uncertainties about homogeneous bandwidths, single-nanocrystal studies can provide insights into carrier trapping and detrapping dynamics. Recent experiments have drawn attention to the possibility that single-NC PL blinking may be linked mechanistically to the phenomenon of delayed luminescence observed in CdSe, Cu^+:CdSe NCs, and related NCs.[31, 35-37] Here, shallow charge trapping can form metastable charge-separated states that de-trap only on very long timescales, leading to extremely slow luminescence decay. In a recent study, we noted the observation of substantial delayed luminescence in $CuInS_2$ NCs that was beyond the scope of that study and hence not described in detail.[15]

Here, we present the first report of single-particle spectra of colloidal $CuInS_2$/CdS core/shell NCs. We show that the PL of single $CuInS_2$/CdS, while being narrower than the ensemble, retains a broad bandwidth, with fwhm ranging from 190-270 meV. Intermittency (blinking) is observed in the single-NC PL time-traces that displays distributed kinetics similar to those of other semiconductor NCs. Interestingly, delayed PL is observed in ensemble measurements on

the same $CuInS_2$/CdS NCs and shows very similar distributed decay kinetics. The blinking and delayed PL dynamics are demonstrated to overlap over a broad experimental time window. Both phenomena are proposed to be attributable to the same reversible carrier-trapping processes. Excitation power-dependence, measured for both prompt and delayed PL in the same experiment, are consistent with the proposed relationship between blinking and delayed PL phenomena. Excitation power dependence shows linearity for the prompt PL versus excitation rate while under the same excitation conditions the delayed PL is sub-linear. This measurement illustrates the major role of excitation rate in determining the ratio of delayed to prompt luminescence, and we propose that this has important consequences at the single particle level.

Results and Analysis

Photoluminescence Spectra and Blinking. Figure 1 summarizes the absorption and PL spectra of $CuInS_2$/CdS NCs. Figure 1A shows absorption and PL spectra of an ensemble of d = 3.8 nm $CuInS_2$/CdS nanocrystals suspended in toluene. The absorption spectrum of the ensemble shows a broad feature centered at ~2.2 eV as the first detectable absorbance, followed by rising absorbance to higher energy. The ensemble PL spectrum shows a broad (fwhm ~ 300 meV) band centered at ~1.65 eV. These ensemble data are very similar to those reported previously for various $CuInE_2$ NCs.[15-19, 21, 25]

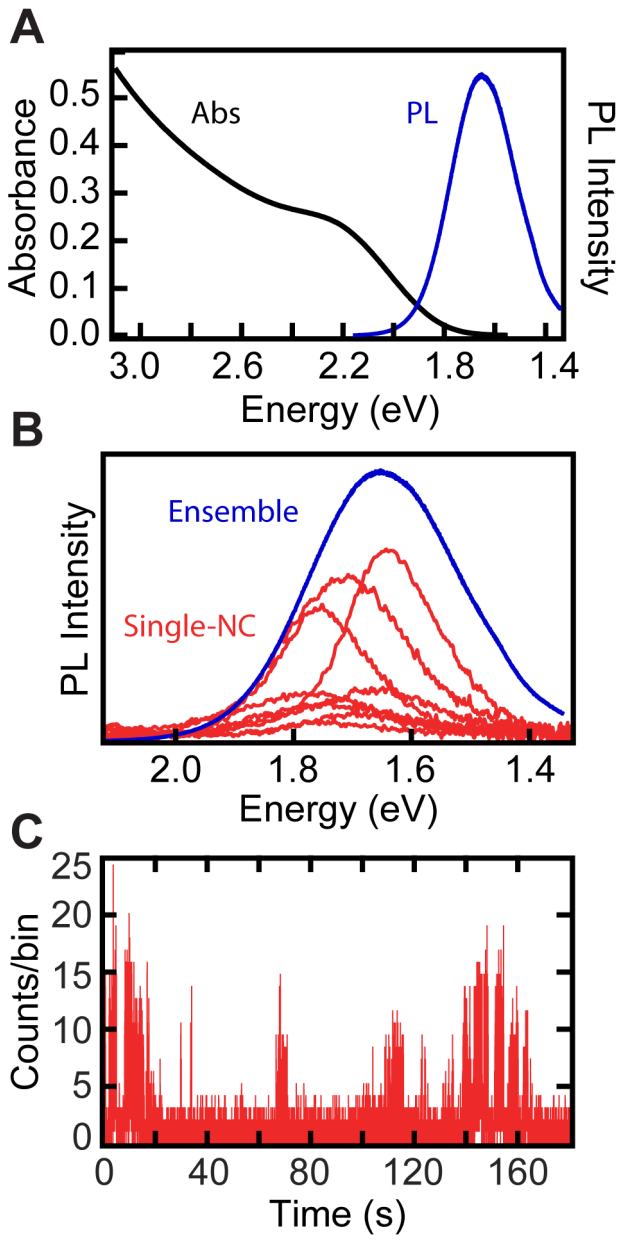

Figure 1. (A) Ensemble absorption and photoluminescence spectra of d = 3.8 nm $CuInS_2$/CdS core/shell NCs in toluene, PL QY = 87%. **(B)** Single-particle and ensemble PL spectra of $CuInS_2$/CdS NCs from the same sample. **(C)** A representative blinking trace from a $CuInS_2$/CdS NC from this same batch (bin size of 7.5 ms). All data were collected at room temperature.

Figure 1B plots the PL spectra of several single nanocrystals from the same ensemble sample as Figure 1A, overlaid with the ensemble PL spectrum. The long PL lifetime of the $CuInS_2$ NCs made acquisition of these single-NC PL spectra challenging, and modification of the nanocrystal

preparation conditions was necessary to achieve reasonable photon counts at the single-particle level (see Methods and Supporting Information). The single-NC spectra in Figure 1B each show a broad PL band, but the fwhm of this band is not the same for all NCs.. Individual spectra range from values as narrow as 190 meV to values up to 270 meV, with no apparent correlation between the PL peak energy and its fwhm (see Supporting Information). These single-NC fwhm values are narrower than the ensemble spectrum (300 meV, Figure 1A), but broad in comparison to excitonic luminescence in II-VI, IV-VI, or related NCs, where room-temperature single-particle bandwidths of ~50 meV are typical[38-40] –indicating some amount of ensemble inhomogeneous broadening. The sum of the single particle spectra shown in Figure 1B appears to be slightly blue-shifted from the ensemble spectrum, a larger statistical sampling is likely needed to recreate the ensemble distribution. Overall, these data illustrate the existence of an effective PL broadening mechanism in individual $CuInS_2$ NCs.

The single-NC PL bandshapes observed here are consistent with the proposal of exciton self-trapping,[15] in which photogenerated holes localize around a single or small group of lattice Cu^+ ions, stabilized by strong electron-phonon coupling. Rather than displaying band-like excitonic emission like in II-VI or III-V NCs, $CuInS_2$ NCs thus more closely resemble high-copper analogs of dilutely Cu^+-doped II-VI and III-V NCs.[15-16] In the Cu^+-doped NCs, single-particle PL bandshapes are broadened by Franck-Condon progressions reflecting vibronic displacement along a combination of lattice contraction and Jahn-Teller distortion coordinates centered at the copper.[41] These distortions are induced by photoexcitation when the copper oxidation state is formally increased from Cu(I) to Cu(II) upon hole localization.[41] Similar lattice distortions are concluded for $CuInS_2$ NCs, although the slightly narrower single-NC PL bandwidths of the $CuInS_2$/CdS NCs compared to Cu^+:CdSe NCs containing single copper dopants[31] (average values

of 235 vs 325 meV respectively) imply slightly shallower hole trapping in the former. While we can't comment on the relative deformability of $CuInS_2$ NCs with respect to other lattices such as CdS; we believe that $CuInS_2$ NCs have larger electron-phonon coupling due to the Jahn-Teller coupling at copper ions that drives the deforming of the lattice and the formation of the self-trapped exciton.

Figure 1C plots a representative PL time trace for one of the single NCs from Figure 1B. PL blinking is readily observed. Blinking data for a total of 88 NCs were analyzed following the Bayesian detection and change-point analysis method outlined by Hess, *et al*.[42] The results of this analysis are discussed below.

Delayed Photoluminescence. Figure 2A presents room-temperature PL decay data measured from the same ensemble of $CuInS_2$/CdS nanocrystals used for Figure 1. The main figure shows a semi-log plot of the first 30 μsec of PL decay data following photoexcitation. The inset shows a log-log plot of the same PL decay, now over 7 orders of magnitude in time. Two clearly separable time regimes are observed in these plots: (*i*) the first ca. microsecond following photoexcitation, in which the majority of the PL decays, and (*ii*) the following period spanning from a few microseconds to over 160 ms (Figure 2A, inset), in which persistent low-level delayed luminescence is observed. The first regime is dominated by "prompt" PL decay with a time constant of $\tau \approx 140$ ns. In contrast, the delayed PL decays non-exponentially, showing broadly distributed kinetics. From these data, we estimate the contribution of delayed PL intensity to the total luminescence intensity to be smaller by a factor of $\sim 5 \times 10^{-3}$. The fraction of delayed to total PL intensities measured *after* the excitation pulse is terminated is much greater. Delayed PL intensities are difficult to determine accurately in the time regime where the prompt PL is dominant, and the widely distributed kinetics make extrapolation unreliable. We therefore

report a lower limit for this factor determined by only counting photons emitted at times longer than 10xτ as delayed PL, where τ is the prompt PL lifetime (140 ns). From this conservative approach, the contribution of delayed to total PL occurring after termination of the excitation pulse is no greater than 10 %. This percentage indicates that the steady-state population of NCs able to eventually emit a delayed photon is quite large, but many of these NCs do not emit delayed luminescence under the steady-state excitation conditions used here.

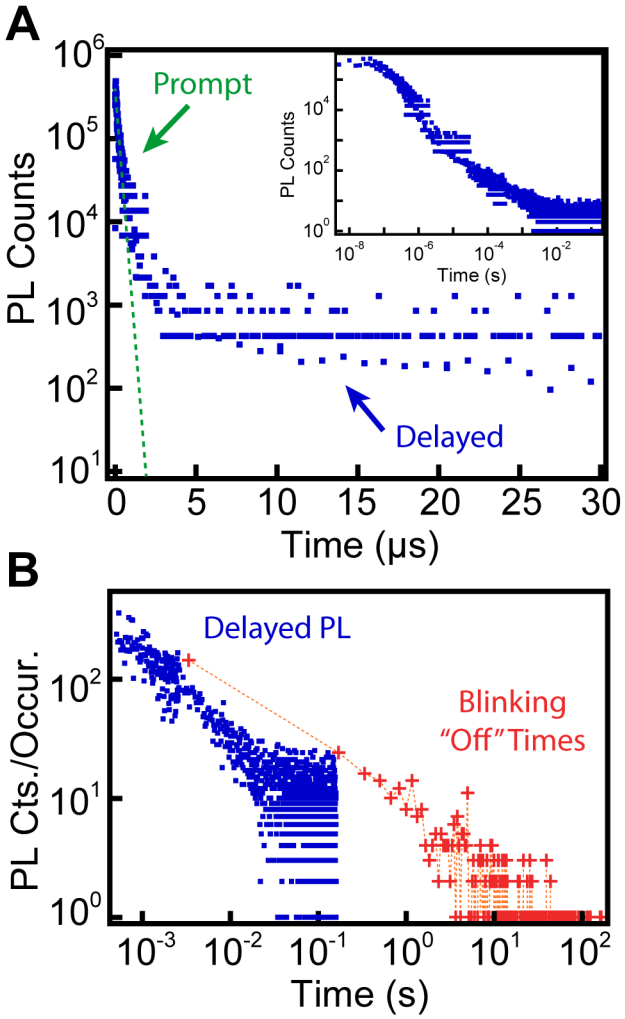

Figure 2. (A) Semi-log plot of PL intensity decay for the same $CuInS_2/CdS$ NCs from Figure 1, showing two distinct time regimes. Prompt luminescence is observed that decays approximately exponentially with a a time constant of $\tau \sim 140$ ns (green dashed curve). Delayed PL is also observed, decaying with distributed kinetics. (Inset) Double-log plot of the same PL decay data, now showing over 7 orders of magnitude in time. Plots were obtained by stitching together multiple time windows with time bins ranging from 5 ns to 10 μs. **(B)** Delayed PL of

$CuInS_2$/CdS NCs (blue squares) and histogram of blinking "off" statistics (red crosses). The blinking data were binned at 1.6 ms for determination of "off" statistics by a Bayesian detection method.[42] The dashed line is a guide to the eye. All data were collected at room temperature.

Figure 2B presents the non-emissive or "off" blinking statistics collected on many single nanocrystals from the same ensemble as used for the delayed luminescence shown in Figure 2A. The red crosses in Figure 2B plot the "off" times for data binned to 1.6 ms and histogrammed with 1000 bins. For comparison, the long-time portion of the delayed PL data from Figure 2A (inset) is also reproduced in Figure 2B. The quantitative intensity scaling for the two experiments is arbitrary because they were performed using different optical systems. Nevertheless, the comparison in Figure 2B illustrates that both the blinking and delayed PL data exhibit similar distributed kinetics that extend over many orders of magnitude in time, and moreover experimentally demonstrates overlapping timescales of the blinking "off" dynamics and the delayed PL decay dynamics. These striking similarities support the hypothesis that these two phenomena are linked mechanistically.[31,35-37]

Photoluminescence Excitation Power Dependence. A key difference between the experimental conditions used for the single-NC blinking and ensemble delayed luminescence measurements shown in Figure 2B is the NC excitation rate. Single-NC PL measurements generally require excitation rates that are several orders of magnitude greater than those typically used for ensemble PL measurements. In this case, the delayed PL data of Figure 2B were collected with an excitation rate of 33 s^{-1}, whereas the blinking data of Figure 2B were collected with an excitation rate of 1.7×10^5 s^{-1} (see Methods). An investigation of the ensemble PL excitation power dependence is therefore informative. Figure 3 summarizes the excitation power dependence of the prompt and delayed PL intensities for the same $CuInS_2$ NCs used in Figures 1 and 2. As illustrated in Figure 3A, NCs were excited using square-wave pulses, allowing

collection of prompt and delayed PL during the "pulse on" and "pulse off" durations of the same experiment, respectively. As demonstrated above, when the excitation pulse is on, the steady-state PL intensity is dominated by the prompt PL, allowing the prompt PL power dependence to be measured directly at steady state. Following termination of the excitation pulse, the total PL intensity decays with the kinetics shown in Figure 2A. The relative power dependence of the delayed PL was measured by integrating from 10-500 μs following the end of the excitation pulse at various excitation powers. The excitation power during the "pulse on" period was tuned to generate average NC excitation rates ranging from k_{exc} = 5 to 80,000 s^{-1}. The lowest excitation rates in this range represent those typical of our ensemble PL measurements, and the highest excitation rates are very similar to those used in our single-NC measurements.

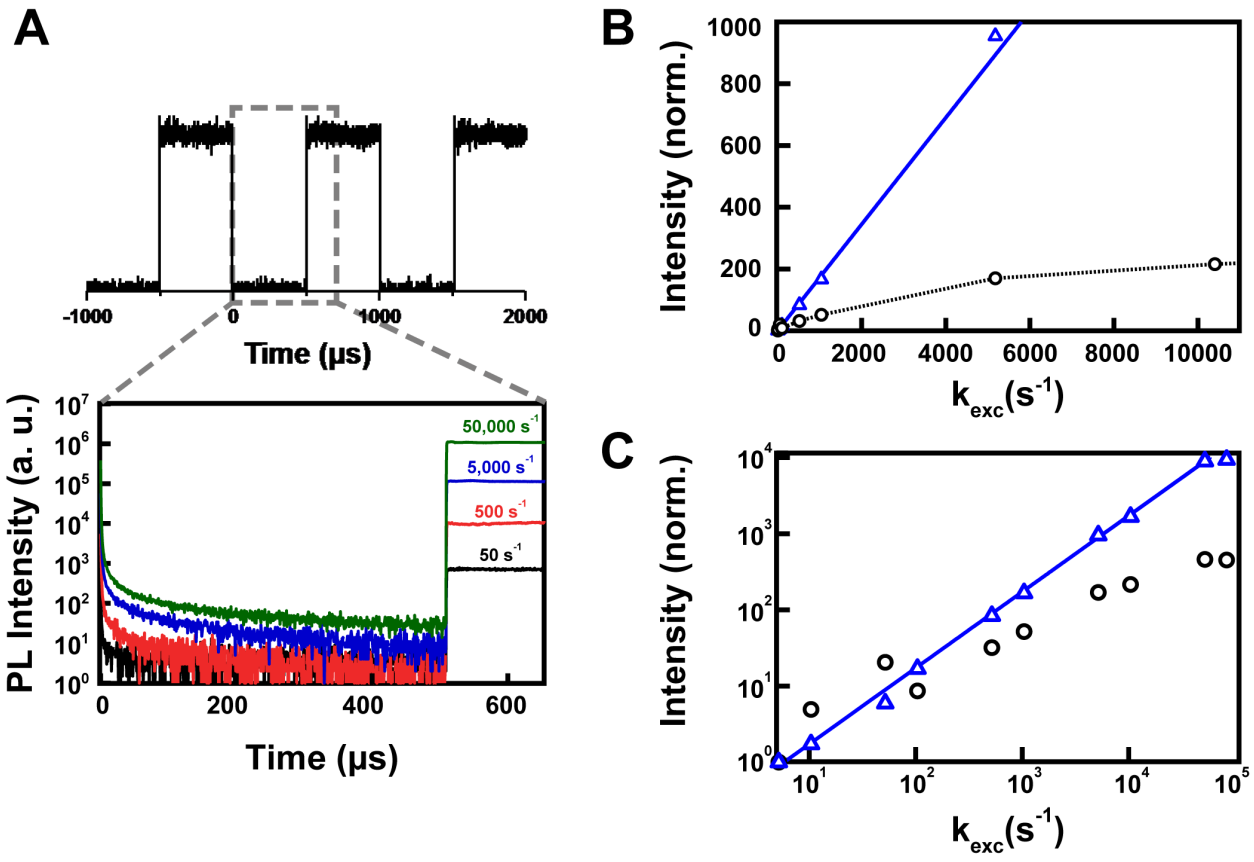

Figure 3. Photoluminescence power dependence measured for the same $CuInS_2$/CdS NCs used for Figures 1 and 2. **(A)** Top: Excitation pulses transmitted through the sample and measured on

a silicon photodiode. The dashed gray box illustrates the time within the pulse train for which PL data were collected. Bottom: PL decay traces measured at 750 nm for selected excitation powers (corresponding to the indicated values of k_{exc}), showing a complete "pulse off" period and the beginning of the next "pulse on" period. **(B)** Plot of the delayed PL intensity measured during a "pulse off" period (black circles) and the prompt PL intensity measured during a "pulse on" period (blue triangles) versus the excitation rate constant (k_{exc}), normalized at k_{exc} = 5 s^{-1}. The delayed PL intensities were obtained by integrating from 10-500 μs after termination of the excitation pulse. The prompt PL intensities were obtained by integrating during the "pulse on" period. The solid blue line represents a linear fit of the prompt PL intensities with the *y*-intercept fixed to the origin. The dashed line is a guide to the eye. **(C)** Double-log plot of the full power-dependence data set (some of which is shown in B), demonstrating linear power dependence of the prompt PL over the entire power range. All data were collected at room temperature. The delayed PL data shown in Figure 2 were measured at

Figure 3B plots the prompt and delayed PL intensities versus excitation power obtained from these measurements, normalized in the low-power limit, *i.e.*, where the steady-state factor of delayed to total PL is ~10^{-3}. The prompt PL intensity increases linearly with increasing excitation rate over the entire range explored here. The reasonably short (~140 ns) lifetime of the prompt PL allows the $CuInS_2$ NCs to cycle quickly between ground and luminescent excited states without saturating, even at the high excitation rates characteristic of the single-NC PL measurements. In contrast, the delayed PL intensity saturates with increasing excitation rate, showing sub-linear power dependence starting even in the low-power regime (k_{exc} ~ 5-500 s^{-1}). Sub-linearity of the delayed PL versus excitation rate implies that recovery of the emissive state is longer than the time between two successive excitation events. The sub-linear delayed-luminescence power dependence evolves over several orders of magnitudes of excitation rates.

Figure 3C plots the full excitation power range in a log-log representation, which highlights the observation that the delayed PL intensity does not fully saturate but instead continues to grow with increasing excitation powers in all power regimes. This continued evolution is a manifestation of distributed relaxation kinetics for the metastable charge-separated state responsible for delayed PL–delayed luminescence involving the longest-lived metastable states

saturating at the lowest excitation powers. Figure 3C shows that the delayed PL is reduced by ~10^2 relative to the prompt PL at the highest excitation powers. The steady-state delayed PL intensity is therefore only ~10^{-5} of the total PL intensity at $k_{exc} = 10^5$ s^{-1}; this excitation rate is close to that used in the single particle blinking measurements. These power-dependence measurements thus predict that formation of the metastable state responsible for delayed luminescence darkens the NC PL by a factor of ~10^5 in the single-NC measurements of Figure 1, *i.e.*, NCs in the metastable state are "off". A consequence of this observation is that in an extremely low hypothetical excitation regime, blinking would not be observed because the emissive state would be recovered from the charge separated state before the next excitation event. However, sub-linearity is observed at excitation rates around 500 s^{-1} for these NCs, which is well below the typical excitation rates used in single particle experiments. More broadly, this observation is highly material dependent and is subject to the QY, prompt lifetime and lifetime of the meta-stable charge separated state of the material being measured, *i.e.*, saturation of a charge separated state and blinking events are material dependent.

Figure 4 summarizes the proposed relationship between delayed luminescence and PL blinking. In the "on" state, NC photoexcitation is followed by radiative recombination to regenerate the NC ground state. For delayed PL, one such photoexcitation event is followed by carrier trapping to generate a metastable charge-separated state. On the basis of our recent studies of Cu^+-doped NCs we assume, for convenience, that the trapped carrier responsible for formation of the metastable charge-separated state is an electron (rather than a hole). However, our proposed mechanistic scheme would be equally valid in the case of a hole trap higher in energy than the copper site.[31] Slow spontaneous detrapping from this metastable state reforms the emissive NC excited state and generates delayed luminescence. The long lifetime of the

metastable charge-separated state allows subsequent photoexcitation of the same nanocrystal to generate a multiply excited NC. A multiply excited NC is more likely to be subject to rapid non-radiative decay, *e.g.*, via Auger or Shockley-Read-Hall-type recombination mechanisms,[43-46] rendering it non-emissive. In other words, the metastable charge-separated state responsible for delayed PL is an "off" state. For convenience, one specific Auger recombination process is illustrated in Figure 4, but other nonradiative processes cannot be excluded. The NC PL remains "off" until these charges recombine. For this reason, the delayed PL dynamics are associated specifically with the NC PL blinking "off" dynamics, as illustrated in Figure 4. Because very similar results are observed for undoped NCs, this general scheme is expected to also apply to excitonic emitters, self-trapped excitons, or other doped NCs such as Cu^{+}:CdSe.

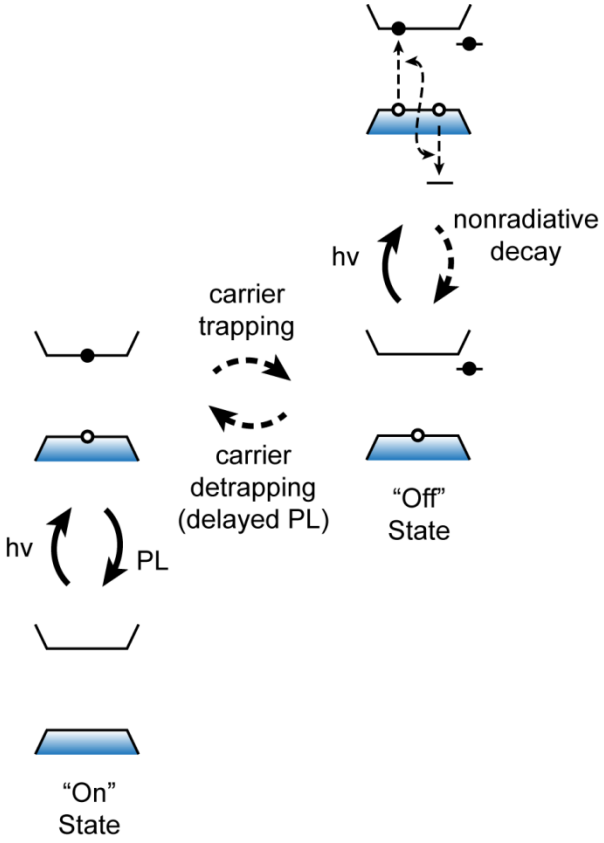

Figure 4. Generalized scheme illustrating the proposed mechanistic link between PL blinking and delayed luminescence in colloidal semiconductor NCs. The dashed arrows denote nonradiative processes and the solid arrows denote radiative processes. Various processes could

possibly contribute to nonradiative decay in the photoexcited "off" state, but for the purposes of illustration here, only one generic Auger recombination process is depicted.

Summary

In summary, single-nanocrystal PL spectra are reported that demonstrate intrinsically broad PL bandshapes in $CuInS_2$ NCs. These bandshapes suggest strong electron-phonon coupling in the emissive excited state of these NCs, consistent with proposals of exciton self-trapping to form a hole-trapped excited state that parallels those of Cu^+-doped semiconductor NCs. In this interpretation, the broad homogeneous bandshapes are determined by Franck-Condon progressions along the lattice distortion coordinates associated with hole contraction in the excited state, and these same distortions generate the characteristically large Stokes shifts of these NCs.

In addition to spectral information, single-NC measurements demonstrate luminescence blinking in individual $CuInS_2$ NCs. A comparison is made between these single-NC blinking statistics and the decay dynamics of delayed luminescence measured on ensembles of the same NCs. The strong similarity between data from these two measurements supports the hypothesis that the "off" state of the blinking phenomenon is identical to the metastable charge-separated state of the delayed luminescence phenomenon. Power-dependence measurements provide additional evidence for the link between delayed luminescence and blinking by showing the likelihood of saturation of the metastable charge-separated state in the delayed PL at the high excitation rates used for blinking, which at the single-NC level would result in the NC being "off" between successive excitation events. A general scheme is presented that illustrates the relationship between these two phenomena in $CuInS_2$ and related colloidal semiconductor NCs.

Methods

Synthesis of $CuInS_2$ nanocrystals. Indium acetate, copper (I) iodide, cadmium nitrate tetrahydrate, myristic acid, sulfur powder, 1-dodecanethiol, and 1-octadecene were purchased from Sigma Aldrich; n-trioctylphosphine was purchased from Strem; sodium hydroxide was purchased from JT Baker. All reagents were used without further purification.

$CuInS_2$/CdS nanocrystals were synthesized by a method adapted from the literature.[19] Briefly, a mixture of indium acetate (0.292 g, 1 mmol), copper iodide (0.190 g, 1 mmol), and dodecanethiol (5 mL) in a 50 mL three-neck round-bottom flask was degassed with three pump-purge cycles at room temperature. The reaction was then heated to 110˚ C under nitrogen and held for 10 min until the solution turned transparent and pale yellow. The reaction was then heated to 230˚ C. The solution turned dark orange at ~220˚C, and was very dark red by 230˚ C. The reaction was held for 10 min at 230˚ C, after which the vessel was cooled rapidly to < 60˚ C.

For CdS shelling, cadmium myristate was prepared by dripping 5 mL of a 0.2 M solution of cadmium nitrate in anhydrous methanol into 30 mL of a 0.1 M solution of myristic acid and sodium hydroxide (0.113 g) in anhydrous methanol. The resulting white precipitate was collected and dried. A shell precursor solution was prepared by heating and sonicating cadmium myristate (0.272 g), sulfur (0.013 g), 1-octadecene (4 mL), and n-trioctylphosphine (0.4 mL) under a nitrogen atmosphere to form a uniform white dispersion.

A portion of the crude reaction solution (1.0 mL) was added to 1-octadecene (4.0 mL) in a clean 50 mL three-neck round-bottom flask. The cores were degassed with three pump-purge cycles using nitrogen at room temperature and were then heated to 210˚ C. The shell precursor solution was injected into the reaction at 0.2 mL/min. After addition of the precursor solution, the reaction was cooled gradually to < 60˚ C. Oleic acid (1 mL) and toluene (1 mL) were then added, and the mixture was stirred for 10 min. The resulting $CuInS_2$/CdS core/shell nanocrystals were purified with several cycles of precipitation with ethanol and centrifugation followed by resuspension in toluene. Samples were characterized by UV-Vis absorption spectroscopy, transmission electron microscopy (see Supporting Information), ensemble photoluminescence, and fluorescence microscopy.

Photoluminescence. Nanocrystals suspended in toluene were excited using a 405 nm diode laser. Photoluminescence was collected perpendicular to the excitation field. A long-pass filter was used to reject any scattered excitation photons, and a monochromator equipped with a LN_2 cooled CCD was used for detection.

Delayed Luminescence. Samples were prepared by sandwiching drop-coated films of nanocrystals between quartz disks. Samples were excited using a 405 nm diode laser at a power density of ~80 mW/cm^2 (k_{exc} ~ 33 s^{-1}) modulated with a pulse waveform output from a function generator. Excitation pulse durations were 50 ms and cycle periods were varied from 55 to 250 ms depending on the time window of interest. PL decay traces were measured at 750 nm using a monochromator equipped with a PMT. Decay traces were collected over multiple time windows from 10 μs to 160 ms. The PMT signal was processed using a multichannel analyzer and collected with a custom LabView program.

Luminescence Excitation Power Dependence. Samples were prepared by sandwiching drop-coated films of nanocrystals between quartz disks. A brass foil with a 230-μm pinhole was mounted on the outsides of the disks, and the samples were placed under vacuum. Excitation was performed through the pinhole to ensure a uniform excitation density. Approximately 60% of the laser Gaussian beam profile (measured by the knife edge technique) was used for excitation. Laser powers were measured prior to the sample and calibrated to account for the ~60% beam transmission. Samples were excited using a 405 nm diode laser with power densities ranging

from 12 mW/cm^2 to 190 W/cm^2, corresponding to per-nanocrystal excitation rates of k_{exc} = 5 – 80,000 s^{-1}. Laser excitation was modulated with a square waveform output from a function generator, with a 1 kHz duty cycle. Emission was measured at 750 nm using a monochromator equipped with a PMT. The PMT signal was processed using a multichannel analyzer and collected using a custom LabView program. Spectra were collected under the same excitation conditions using the same monochromator and a LN_2 cooled CCD.

Single-Particle Luminescence. Extensive optimization of the conditions for single particle measurements was necessary to minimize the apparent decrease in PL QY of the $CuInS_2$/CdS NCs upon deposition onto the substate. This optimization process included many attempts to embed NCs in various polymers, and finally resulted in the elimination of polymer and addition of decanethiol upon dilution to (presumably) provide a suitable ligand environment for the NCs at the very small concentrations required for single-particle measurements. $CuInS_2$/CdS nanocrystals (~100 μM) were diluted by a factor of 200 into a solution of 9 parts toluene to 1 part dodecanethiol and then sonicated. The resulting solutions were then diluted in chloroform by a factor of 20,000 to give a final dilution factor of 400,000. The solutions were then spin coated onto cleaned zinc titania glass cover slips at 2000 rpm. The samples were mounted on an xy-piezoelectric nano-positioning stage (PI, P-545.2R7) in an inverted confocal microscope (Nikon, TE2000U). Single-particle experiments were performed under flowing N_2. Photoexcitation was accomplished using a 470 nm pulsed picosecond diode laser (PicoQuant, PDL 800-B with LDH-P-C-405B laser head) with a pulse width of 63 ps (full-width at half-maximum), repetition rate of 5 MHz, and an average power of 90 nW (measured at the focal point of the objective). Assuming a diffraction-limited focal point, this excitation power gives an upper bound photon absorption cross section of 0.037 photons per pulse, corresponding to an excitation rate of 1.7x10^5 s^{-1}. A 562 nm dichroic long-pass mirror directed the excitation field to the back of a 100x oil-immersion objective (1.4 NA) where it was focused through the glass coverslip to a diffraction-limited spot. Luminescence was collected in an epi-geometry, passed through the 562 nm dichroic long-pass mirror and then passed through a second long-pass filter to reject scatter from the photoexcitation field. Luminescence was then split by a 50/50 beam splitter, with the transmitted and reflected fields focused onto two separate avalanche photodiode detectors (APD) with 50 μm active areas providing confocal resolution. Observation of single-step photobleaching events, diffraction-limited spot sizes, and a dependence of emission spots per area on nanocrystal concentration confirm measurement of single nanocrystals. Microscope and collection-electronics were controlled using a custom LabView program.

Luminescence spectra of single $CuInS_2$/CdS nanocrystals were measured on the same spin coated films used for the luminescence blinking studies and using the same microscope. The luminescence was focused onto a 100 μm pinhole to achieve confocal resolution and then delivered to a monochromator equipped with a LN_2 cooled CCD. Spectra were collected with 300 sec exposures, 5 MHz rep rate, and 90 nW average excitation power.

Acknowledgments. Financial support from the National Science Foundation (CHE-1404674 to P.J.R. and DMR-1505901 to D.R.G.) is gratefully acknowledged. K.E.K. thanks the Department of Energy for support through an Energy Efficiency and Renewable Energy (EERE) postdoctoral research award. A. M. acknowledges the support of an Early Postdoc Mobility Fellowship from the Swiss National Science Foundation.

References

(1) Aldakov, D.; Lefrançois, A.; Reiss, P., *J. Mater. Chem. C* **2013,** *1*, 3756.
(2) Yu, K.; Ng, P.; Ouyang, J.; Zaman, M. B.; Abulrob, A.; Baral, T. N.; Fatehi, D.; Jakubek, Z. J.; Kingston, D.; Wu, X.; Liu, X.; Hebert, C.; Leek, D. M.; Whitfield, D. M., *ACS Appl. Mater. Interfaces* **2013,** *5*, 2870.
(3) Leach, A. D.; Macdonald, J. E., *J. Phys. Chem. Lett.* **2016,** *7*, 572.
(4) Chen, C.-W.; Wu, D.-Y.; Chan, Y.-C.; Lin, C. C.; Chung, P.-H.; Hsiao, M.; Liu, R.-S., *J. Phys. Chem. C* **2015,** *119*, 2852.
(5) Chuang, P. H.; Lin, C. C.; Liu, R. S., *ACS Appl. Mater. Interfaces* **2014,** *6*, 15379.
(6) Knowles, K. E.; Kilburn, T. B.; Alzate, D. G.; McDowall, S.; Gamelin, D. R., *Chem. Commun. (Cambridge)* **2015,** *51*, 9129.
(7) Meinardi, F.; McDaniel, H.; Carulli, F.; Colombo, A.; Velizhanin, K. A.; Makarov, N. S.; Simonutti, R.; Klimov, V. I.; Brovelli, S., *Nat. Nanotechnol.* **2015,** *10*, 878.
(8) Li, C.; Chen, W.; Wu, D.; Quan, D.; Zhou, Z.; Hao, J.; Qin, J.; Li, Y.; He, Z.; Wang, K., *Sci. Rep.* **2015,** *5*, 17777.
(9) Yoshino, K.; Ikari, T.; Shirakata, S.; Miyake, H.; Hiramatsu, K., *Appl. Phys. Lett.* **2001,** *78*, 742.
(10) Tell, B.; Shay, J. L.; Kasper, H. M., *Phys. Rev. B* **1971,** *4*, 2463.
(11) Yakushev, M. V.; Mudryi, A. V.; Victorov, I. V.; Krustok, J.; Mellikov, E., *Appl. Phys. Lett.* **2006,** *88*, 011922.
(12) Binsma, J. J. M.; Giling, L. J.; Bloem, J., *J. Lumin.* **1982,** *27*, 35.
(13) Ueng, H. Y.; Hwang, H. L., *J. Phys. Chem. Sol.* **1989,** *50*, 1297.
(14) Ueng, H. Y.; Hwang, H. L., *J. Phys. Chem. Sol.* **1990,** *51*, 1.
(15) Knowles, K. E.; Nelson, H. D.; Kilburn, T. B.; Gamelin, D. R., *J. Am. Chem. Soc.* **2015,** *137*, 13138.
(16) Knowles, K. E.; Hartstein, K. H.; Kilburn, T. B.; Marchioro, A.; Nelson, H. D.; Whitham, P. J.; Gamelin, D. R., *Chem. Rev.* **2016,** *Article ASAP*.
(17) Castro, S. L.; Bailey, S. G.; Raffaelle, R. P.; Banger, K. K.; Hepp, A. F., *J. Phys. Chem. B* **2004,** *108*, 12429.
(18) Nakamura, H.; Kato, W.; Uehara, M.; Nose, K.; Omata, T.; Otsuka-Yao-Matsuo, S.; Miyazaki, M.; Maeda, H., *Chem. Mater.* **2006,** *18*, 3330.
(19) Li, L.; Pandey, A.; Werder, D. J.; Khanal, B. P.; Pietryga, J. M.; Klimov, V. I., *J. Am. Chem. Soc.* **2011,** *133*, 1176.
(20) Zhong, H.; Zhou, Y.; Ye, M.; He, Y.; Ye, J.; He, C.; Yang, C.; Li, Y., *Chem. Mater.* **2008,** *20*, 6434.
(21) Xie, R.; Rutherford, M.; Peng, X., *J. Am. Chem. Soc.* **2009,** *131*, 5691.
(22) Omata, T.; Tani, Y.; Kobayashi, S.; Otsuka-Yao-Matsuo, S., *Thin Solid Films* **2012,** *520*, 3829.
(23) Chen, B.; Zhong, H.; Zhang, W.; Tan, Z. a.; Li, Y.; Yu, C.; Zhai, T.; Bando, Y.; Yang, S.; Zou, B., *Adv. Funct. Mater.* **2012,** *22*, 2081.
(24) Liu, W.; Zhang, Y.; Zhao, J.; Feng, Y.; Wang, D.; Zhang, T.; Gao, W.; Chu, H.; Yin, J.; Wang, Y.; Zhao, J.; Yu, W. W., *J. Lumin.* **2015,** *162*, 191.
(25) Sun, J.; Ikezawa, M.; Wang, X.; Jing, P.; Li, H.; Zhao, J.; Masumoto, Y., *Phys. Chem. Chem. Phys.* **2015,** *17*, 11981.
(26) Tran, T. K. C.; Le, Q. P.; Nguyen, Q. L.; Li, L.; Reiss, P., *Adv. Nat. Sci.: Nanosci. Nanotechnol.* **2010,** *1*, 025007.

(27) Hamanaka, Y.; Kuzuya, T.; Sofue, T.; Kino, T.; Ito, K.; Sumiyama, K., *Chem. Phys. Lett.* **2008,** *466*, 176.
(28) Uehara, M.; Watanabe, K.; Tajiri, Y.; Nakamura, H.; Maeda, H., *J. Chem. Phys.* **2008,** *129*, 134709.
(29) Omata, T.; Nose, K.; Kurimoto, K.; Kita, M., *J. Mater Chem. C* **2014,** *2*, 6867.
(30) Shabaev, A.; Mehl, M. J.; Efros, A. L., *Phys. Rev. B* **2015,** *92*, 035431.
(31) Whitham, P. J.; Knowles, K. E.; Reid, P. J.; Gamelin, D. R., *Nano Lett.* **2015,** *15*, 4045.
(32) Brovelli, S.; Galland, C.; Viswanatha, R.; Klimov, V. I., *Nano Lett.* **2012,** *12*, 4372.
(33) Ishizumi, A.; White, C. W.; Kanemitsu, Y., *Appl. Phys. Lett.* **2004,** *84*, 2397.
(34) Zhang, A.; Dong, C.; Li, L.; Yin, J.; Liu, H.; Huang, X.; Ren, J., *Sci. Rep.* **2015,** *5*, 15227.
(35) Sher, P. H.; Smith, J. M.; Dalgarno, P. A.; Warburton, R. J.; Chen, X.; Dobson, P. J.; Daniels, S. M.; Pickett, N. L.; O'Brien, P., *Appl. Phys. Lett.* **2008,** *92*, 101111.
(36) Rabouw, F. T.; Kamp, M.; van Dijk-Moes, R. J.; Gamelin, D. R.; Koenderink, A. F.; Meijerink, A.; Vanmaekelbergh, D., *Nano Lett.* **2015,** *15*, 7718.
(37) Rabouw, F. T.; van der Bok, J. C.; Spinicelli, P.; Mahler, B.; Nasilowski, M.; Pedetti, S.; Dubertret, B.; Vanmaekelbergh, D., *Nano Lett.* **2016,** *16*, 2047.
(38) Yu, W. W.; Qu, L.; Guo, W.; Peng, X., *Chem. Mater.* **2003,** *15*, 2854.
(39) Reiss, P.; Bleuse, J.; Pron, A., *Nano Lett.* **2002,** *2*, 781.
(40) Mekis, I.; Talapin, D. V.; Kornowski, A.; Haase, M.; Weller, H., *J. Phys. Chem. B* **2003,** *107*, 7454.
(41) Nelson, H. D.; Li, X.; Gamelin, D. R., *J. Phys. Chem. C* **2016,** *120*, 5714.
(42) Hess, C. M.; Riley, E. A.; Reid, P. J., *J. Phys. Chem. B* **2014,** *118*, 8905.
(43) Rosen, S.; Schwartz, O.; Oron, D., *Phys. Rev. Lett.* **2010,** *104*, 157404.
(44) Zhao, J.; Nair, G.; Fisher, B. R.; Bawendi, M. G., *Phys Rev Lett* **2010,** *104*, 157403.
(45) Galland, C.; Ghosh, Y.; Steinbruck, A.; Sykora, M.; Hollingsworth, J. A.; Klimov, V. I.; Htoon, H., *Nature* **2011,** *479*, 203.
(46) Rinehart, J. D.; Schimpf, A. M.; Weaver, A. L.; Cohn, A. W.; Gamelin, D. R., *J. Am. Chem. Soc.* **2013,** *135*, 18782.